# Fabrication of a flexible stretchable hydrogel-based antenna using a femtosecond laser for miniaturization

## PINGPING ZHAO, TAO CHEN, 1, JINHAI SI, HONGYU SHI, 2 D AND Xun Hou<sup>1</sup>

<sup>1</sup> Key Laboratory of Physical Electronics and Devices of the Ministry of Education & Shaanxi Key Lab of Information Photonic Technique, School of Electronic Science and Engineering, Faculty of Electronic and Information Engineering, Xi'an Jiaotong University, Xi'an, Shaanxi 710049, China

**Abstract:** We demonstrated a new method of fabricating a stretchable antenna by injecting liquid metal (LM) into a femtosecond-laser-ablated embedded hydrogel microchannel, and realized miniaturization of a stretchable dipole antenna based on hydrogel substrate. Firstly, symmetrical microchannels with two equal and linear branches were formed by a femtosecond laser in the middle of a hydrogel substrate, and then were filled with LM by use of a syringe needle. Using this method, a stretchable LM-dipole antenna with each dimension of  $24 \text{ mm} \times 0.6$ mm  $\times$  0.2 mm separated by a 2-mm gap, was formed in the middle of a 70 mm  $\times$  12 mm  $\times$  7 mm hydrogel slab. Since the polyacrylamide (PAAm) hydrogel contained ~ 95 wt % deionized water with a high permittivity of 79 in the 0.5 GHz - 1.5 GHz range, the hydrogel used to prepare the flexible antenna can be considered as distilled water boxes. Experiments and simulations showed that a 5-cm-long LM-dipole embedded in hydrogel resonated at approximately 927.5 MHz with an S<sub>11</sub> value of about - 12.6 dB and omnidirectional radiation direction. Benefiting from the high permittivity of the hydrogel, the dipole length was downsized by about half compared with conventional polymer substrates at the same resonant frequency. By varying the applied strain from 0 to 48%, the resonant frequency of the hydrogel/LM dipole antenna can be tuned from 770.3 MHz to 927.0 MHz. This method provides a simple and scalable technique for the design and preparation of LM-pattern microstructures in hydrogels, and has potential applications in hydrogel-based soft electronic device.

© 2023 Optica Publishing Group under the terms of the Optica Open Access Publishing Agreement

#### 1. Introduction

The proliferation of wireless technologies and the Internet of Things has necessitated the development of communication technologies to meet the requirements of the next generation systems and support other multiband and multistandard wireless systems [1–3]. The technologies acceleration has driven the hardware to be more compact, easier to integrate, and more economic while offering smarter and more multifunctional characteristics [4–7]. With the increasing popularity of flexible electronic devices and the rapid development of wireless communication technology, flexible antennas represent an essential link between soft electronics and external systems for control, power delivery, data processing, and/or communication [8–10]. Stepping forward from traditional rigid electrodes, stretchable and miniaturized antennas offer a unique potential to interface with human skin or soft biological materials while communicating between the sensors and users [11–13]. The resonant frequency  $(f_0)$  of the stretchable antenna can be mechanically tuned by elongating, and can therefore act as a wireless strain sensor [14,15]. The key factors in developing stretchable and miniaturized antennas are the materials and integrated systems needed to retain structurally and functionally intact while stretching. This requires a

<sup>&</sup>lt;sup>2</sup>School of Information and Communications Engineering, Xi'an Jiaotong University, Xi'an 710049, China \*tchen@mail.xjtu.edu.cn

devotion to designing both the substrates and electrode materials, typically involving a demanding set of considerations in performance, size, and stretchability. A lot of effort has been invested over the past several years to improve the performance parameters of the antenna, such as metamaterial [16–19] and metasurfaces [20,21]. Moreover, a wide variety of flexible antennas consisting mainly of flexible substrates and conductive materials have been reported, such as monopole antenna [22], dipole antenna [23], loop antenna [24], coil antenna [25], patch antenna [26], and spiral antenna [27]. Among various flexible substrate materials, the hydrogel has attracted widespread attention for its excellent biocompatibility, mechanical properties similar to biological tissues, and adjustable physicochemical properties. It has been used as a substrate for flexible antennas, such as near-field communication antenna [28,29], RFID tag antenna [30], patch antenna [31], and wireless inductive sensing [32]. The conductive materials commonly used in flexible electronics mainly include solid metal, carbon nanotube, ionic liquid, and liquid metal (LM). Among them, metal [33,34] is prone to partial layering and cracking due to its mechanical mismatch with flexible substrates, while carbon nanotube [35] and ionic liquid [36] have high power consumption due to their high resistance. In contrast, LM become a popular candidate due to its high conductivity, flowability, and filling ability [37]. More importantly, LM conductive pattern is suitable for manufacturing inductors [38,39], which is difficult for ionic conductors. Therefore, LM patterning in the hydrogel is an indispensable step for the preparation of stretchable and wireless electronics such as stretchable antennas.

Recently, tremendous efforts have been made in LM conductive pattern on hydrogels and other flexible substrates, such as direct ink writing [40], stencil printing [41,42], masked deposition [43,44], 3D printing [45,46], and microfluidic injection [47–49]. The above writing, printing, and deposition methods allow customized two-dimensional delicate LM patterns on hydrogels, but additional films may be employed to encapsulate them. 3D printing allows LM-patterns to be suspended in hydrogels, but is limited by the supporting medium hydrogels. Although microfluidic injection creates LM-spiral structures by injecting LM into microchannels formed by screwing springs in/out hydrogels [47], customization of 3D LM patterns embedded in hydrogels remains challenging. The rapidly developing femtosecond laser has become a powerful tool for direct writing of 3D microchannels [50] and metal microstructures [51]. 3D LM microcomponents were achieved by injecting LM into complex 3D microchannels/cavities formed in fused silica using femtosecond laser irradiation followed by chemical etching technology, which could be served as micromoulds of the metallic microcomponents. Moreover, the femtosecond laser takes advantage of high-resolution processing and high-precision control in direct writing 3D embedded hydrogel microchannels [52]. However, the hydrogel/LM micro-structures fabricated by injecting LM into femtosecond-laser-ablated embedded hydrogel microchannels and their application in antenna remain to be further investigated.

In addition, antenna miniaturization techniques have received attention and in-depth research in integrated systems for wireless communication and/or operation [53,54], such as increasing the effective resonant length in limited space [55], improving impedance matching [56], and increasing the permittivity ( $\epsilon$ ) of the substrates [57]. Among them, using a high- $\epsilon$  substrate can reduce the working wavelength of the antenna in the dielectric material, and shorten the resonant length of the antenna at the same  $f_0$ . This approach does not increase the complexity of the antenna structure, and can also collaborate with other technologies, which is essential for the miniaturization of antennas. Inui *et al.* printed a miniaturized flexible dipole antenna on a high- $\epsilon$  silver nanowire/nanopaper composite substrate [58]. The silver antenna printed on this substrate ( $\epsilon$  = 726.5 at 1.1 GHz) was downsized by about a half, compared with the antenna printed on the original nanopaper ( $\epsilon$  = 5.3) or conventional polymer substrates such as polyethylene terephthalate ( $\epsilon$  = 3.1), polyethylene naphthalate ( $\epsilon$  = 3.4), polyimide ( $\epsilon$  = 3.4), silicone ( $\epsilon$  = 2.8) [59], and polydimethylsiloxane (PDMS) ( $\epsilon$  = 2.5) [60]. Although paper substrate can be bent, its stretchability is small. Gels and gel-derived materials are not only stretchable,

but their dielectric property can also be precisely tuned over a wide range due to the diversity and stability of the liquids. Guo *et al.* synthesized high- $\varepsilon$  and stretchable dielectric gels for improving the sensitivity of capacitive sensors, and the gel  $\varepsilon$  value is about 34 to 30 at the range of frequency from 1 kHz to 1 MHz [61]. Zhao *et al.* concluded that water-rich hydrogel with low monomer concentration exhibits high- $\varepsilon$  prepared by employing the co-contribution of dielectrically inert polymer networks and liquids [62]. They selected the typical soft polymeric acrylamide (AM) as the monomer because of its good compatibility with many liquids and abundant intra-, intermolecular hydrogen bonds, forming polyacrylamide abbreviated as PAM or PAAm chains that completely disperse in non-aggregated states in water. However, the impact of its high- $\varepsilon$  on hydrogel-based antenna  $f_0$  remains further research.

In this paper, we propose a new method of fabricating a stretchable antenna by injecting LM into femtosecond-laser-ablated embedded hydrogel microchannels, and realize miniaturization of stretchable dipole antenna based on hydrogel substrate. The resonant and radiation characteristics of hydrogel/LM dipole antenna are studied by experimental measurement and simulation. The influences of antenna size were investigated. In addition, the stretchability and tunability of the hydrogel/LM dipole antenna were demonstrated.

#### 2. Materials and methods

#### 2.1. Fabrication of LM-pattern in hydrogel microchannels

We prepared PAAm hydrogel as a demonstration, following the method of Gao *et al.* [63]. Firstly, 30 ml aqueous solution of AM (monomer; 3.0 M, 6.399 g), methylene bisacrylamide (crosslinker; 0.2 mol%, 0.027 g), and ammonium persulfate (initiator; 0.05 mol%, 0.009 g) were mixed in a plastic beaker. Then, the solution was pipetted to fill a volume between two parallel glass sheets separated by a silicone spacer, the thickness of which limited the hydrogel thickness. After gelation at 60 °C for 6 h, the PAAm gel membrane was synthesized and peeled off from the substrate. Finally, the formed PAAm gels were immersed in deionized (DI) water for more than 24 h to allow complete swelling.

Figure 1 shows a schematic of the experimental setup and procedure for fabricating LM patterns in hydrogel microchannels. The experimental setup mainly consists of light source, electronically controlled three-axis translation stage, microscope system, and charge-coupled device (CCD) image sensor as shown in Fig. 1(a). The laser source was a Ti:sapphire regenerative amplifier (Libra-USP-HE, Coherent Inc., USA), which delivered a train of 800 nm, 50 fs laser pulses at 1 kHz repetition rate. The laser beam passed through the optical components into the microscope system (Nikon, Eclipse LV 100D), then focused into the hydrogel sample via a  $50\times$  microscope objective (Olympus, NA = 0.5), and the power was adjusted by a variable attenuator. Due to its ultrashort pulses and ultrahigh peak power, the focused femtosecond laser pulse can precisely form embedded hollow microchannels based on multiphoton absorption without affecting the hydrogel surface. In order to prevent the shrinkage of the hydrogel while fabricating microchannels, the hydrogel was covered with a thin cover glass with a thickness of 120  $\mu$ m and aligned with the DI water surface in the petri dish. The motion of the entire dish was controlled by a three-axis translation stage that is mounted on a microscope system.

Figure 1(b) shows the process of preparing a hydrogel/LM dipole antenna, including the microchannel fabrication and LM injection. First, the laser beam was focused into half of the hydrogel thickness and scanned multiple times to form symmetrical hydrogel microchannels with two equal and linear branches separated by a 2-mm gap. Then, two reservoirs were inscribed at each of the microchannel adjacent ends for the connection of coaxial connector (SMA) pins in subsequent experiments, and the microchannels were scanned once from each microchannel for air circulation. After laser inscription, superconductive LM (EGaIn, 75% Ga, 25% In,  $\sigma = 2.8 \times 10^6$  S/m), a room temperature liquid-phase eutectic [64], was employed to serve as the conductive element filling the hydrogel microchannels by a syringe needle with a diameter of  $\sim$ 

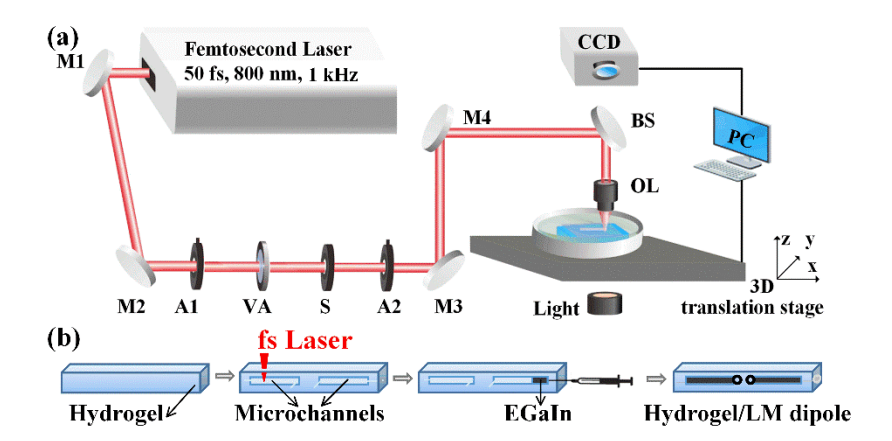


**Fig. 1.** Schematic of experimental setup and procedure for fabricating LM patterns in hydrogel microchannels. (a) Fabrication and microscope system - M1, M2, M3, M4: reflector; A1, A2: continuously variable irises; VA: variable attenuator; S: shutter; BS: beam splitter; OL: objective lens; CCD: charge-coupled device image sensor. (b) The procedure of a hydrogel/LM dipole antenna.

0.2~mm. Since LM is not hydrophilic, the water [65] in the hydrogel microchannels prevents the LM's surface oxides [66] from adhering to microchannel walls, thus reducing the pressure required [67,68] for LM to flow therein. This allows the LM to slide along the microchannel and reach certain areas, thus forming LM patterns with dipole microstructures. After removing the needle, the microchannel entrances were sealed with ethyl  $\alpha$ -cyanoacrylate. Finally, a flexible dipole antenna consisting of two equal, linear LM branches separated by a 2-mm gap in the hydrogel was prepared.

## 2.2. Electromagnetic characterization of hydrogel/LM antenna

The electromagnetic characteristics of antennas mainly include the frequency and direction characteristics, which determine the basic functions of energy conversion and radiation direction. A vector network analyzer (Agilent E8363B) was applied for measuring the frequency and corresponding reflection coefficients of antennas in the free space. The antenna radiation patterns (H and E plane) around resonated frequency are measured in the anechoic chamber. To mitigate the effects of the connector and propagation loss while measuring, the dipole antenna is excited using the model of commercially available SMA connector and fed by a coaxial cable. The basic structure of a coaxial cable consists of an inner cylindrical conductor in the center, an outer braided mesh conductor in a ring-shape, an insulation separating the two conductors, and a protective sheath. When a coaxial cable feeds an antenna, the signal is transmitted from the inner conductor and returned from the outer conductor through the insulation layer. This forms a current loop between the two conductors that constrains the electromagnetic waves in it, thus guiding them transmitted along the coaxial cable without leaking into the external environment. In terms of coaxial cable feed dipole antenna, the coaxial probe is generally connected to one branch and located in the center of the dipole. In our experiment, the SMA connector with a 2-mm gap was inserted into the reservoirs through a plastic sheet used for fixing interface adhesion to connect with the LM-dipole branches, and sealed with ethyl α-cyanoacrylate between SMA and hydrogel.

The vector network analyzer transmits incident electromagnetic waves of different frequencies from the internal signal source of port 1 into the antenna through the coaxial cable and the SMA connector. The electromagnetic waves are partly radiated around the antenna and partly returned

by the antenna to the receiver in port 1 through the coaxial cable. The reflection coefficient  $\Gamma$  is the ratio of the reflected voltage of the antenna to the transmitted voltage of the signal source, measured and calculated by the network analyzer to get the reflection coefficient  $S_{11}$  curve. It is common to express the reflection coefficient in decibels (dB), using the expression 20 log  $|\Gamma|$ , also known as return loss. A low value of  $S_{11}$  indicates less antenna reflection, which means the antenna matches the source impedance. The  $S_{11}$  values below - 10 dB are generally expected effective, while small electronics can be considered valid at - 6 dB [69]. When the antenna reaches the lowest  $S_{11}$  value at a specific frequency,  $S_{11}$  increases rapidly when it deviates from the specific frequency, called  $f_0$ . In anechoic chamber, the antenna sample is placed on a turntable at the same height as the standard antenna. The turntable is controlled to rotate the sample in the horizontal plane to measure the field intensity at different angles. The antenna is placed horizontally and vertically on the turntable, and its field intensity is measured in the E and H plane. After normalization, the E-plane and H-plane radiation patterns of the antenna sample are obtained in the polar coordinate.

#### 3. Results and discussion

## 3.1. Fabrication and characterization of hydrogel/LM dipole antenna

The dielectric properties of the PAAm hydrogel used to prepare the flexible antenna in this paper were tested with a sweep signal from 0.5 GHz to 18 GHz using a network analyzer (Keysight N5222A). The hydrogel slab samples with 70 mm × 12 mm × 7 mm was sandwiched by two copper electrodes. By calculating the ratio of the weight difference between the hydrogel and the dehydrated hydrogel to the weight of the hydrogel, the water content of the hydrogel is about 95 wt %. The permittivity of hydrogel, dehydrated hydrogel and DI water were measured as shown in Fig. 2. It can be seen that the hydrogel permittivity is proximity to that of DI water, much higher than that of dehydrated hydrogel. The hydrogel permittivity decreases from 80 to 40 when the frequency increases from 0.5 GHz to 18 GHz. The hydrogel permittivity is 79 at 0.9 GHz, much higher than the dehydrated hydrogel of 3, which is proximity to that of common flexible substrate materials [59,60]. Since the PAAm hydrogel contain a large amount of water with 95 wt %, its high permittivity mainly be attributed to DI water. Therefore, the PAAm hydrogel slab used to prepare the flexible antenna can be considered as distilled water boxes.

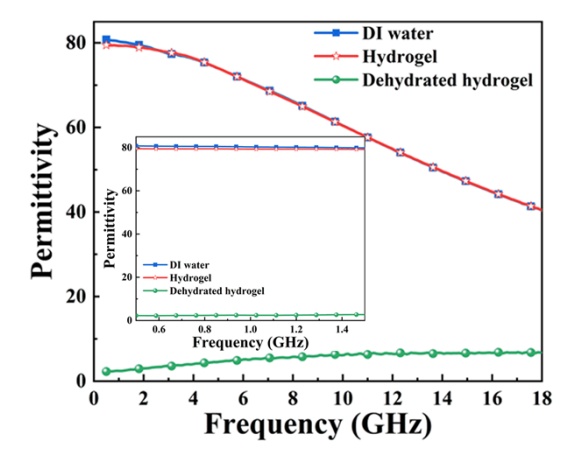


**Fig. 2.** The relative permittivity of the synthesized PAAm hydrogel at a range of frequency from 0.5 GHz to 18 GHz.

The process of fabricating the hydrogel/LM dipole antenna shown in Fig. 1(b) was started by multiple-time scanning by femtosecond laser direct writing (FLDW). The femtosecond laser

power and scanning speed were set at 60 mW and 500  $\mu$ m/s, respectively. A 24-mm long microchannel was produced in the hydrogel by the electronically controlled three-axis translation stage moving at a constant speed during femtosecond laser irradiation and monitored in real-time using a CCD. Since the microchannel width formed by a single scan of the femtosecond laser is only tens of micrometers, the femtosecond laser is translated 15  $\mu$ m along the longitudinal direction after each scan and repeated 40 times to broaden the microchannels with a width of 600  $\mu$ m. As a result, a pair of horizontal microchannels of 24 mm×0.6 mm×0.2 mm with a 2-mm gap was formed by FLDW repeatedly 40 times in the middle of a 70 mm×12 mm×7 mm hydrogel slab, and two 1 mm×1 mm reservoirs were respectively formed at the two adjacent ends of the microchannels for SMA connector access shown in Fig. 3(a). After LM injection, the top and bottom views of the dipole antenna were shown in Fig. 3(b) and 3(c), respectively. In addition, a sample of hydrogel microchannel with the same dimensions but without LM was prepared for comparison experiments.

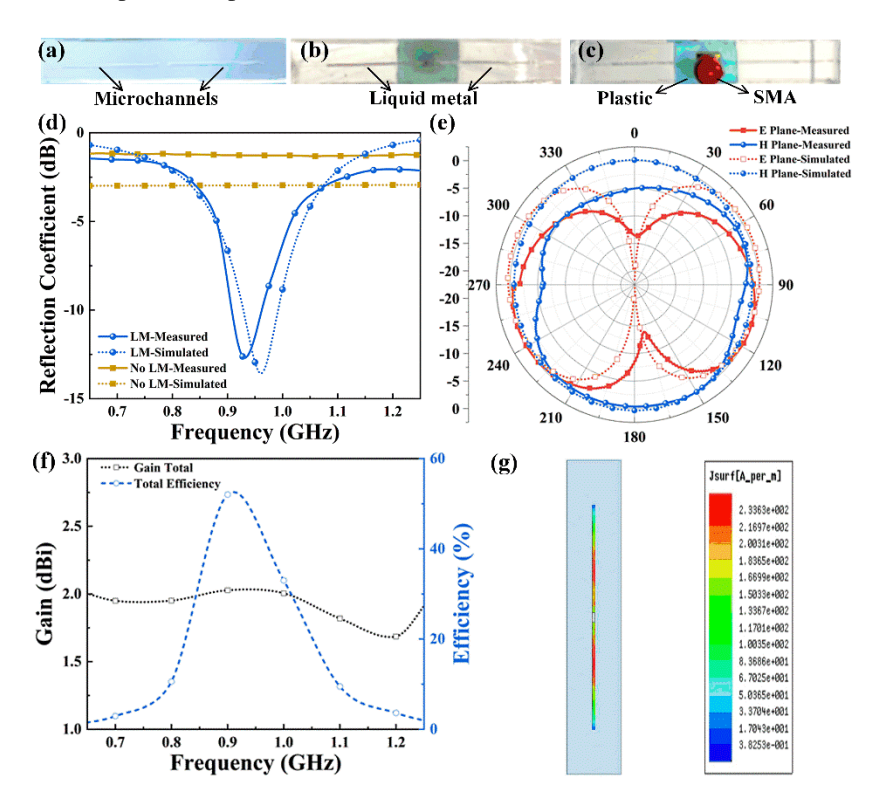


**Fig. 3.** Fabrication and characterization of a hydrogel/LM dipole antenna. (a) Two horizontal microchannels of 24 mm  $\times$  0.6 mm  $\times$  0.2 mm with a 2-mm gap were symmetrically inscribed in the middle of the hydrogel slab. The laser power and scanning speeds were set to 30 mW and 500 µm/s, respectively. (b) Top and (c) bottom views of LM/hydrogel dipole antenna. (d) Reflection coefficient  $S_{11}$ . (e) Measured and simulated normalized radiation pattern in the E-plane and H-plane at 0.9 GHz. (f) Simulated gain and efficiency performance. (g) Surface current density at 0.9 GHz.

We characterized the frequency and direction properties of the dipole antenna in the free space. Accordingly, the antenna's response to electromagnetic waves excited at different frequencies was computed in Ansys High Frequency Structure Simulator (HFSS). In HFSS 15.0, superconducting LM and hydrogel are considered perfect conductors (PEC) sheets with infinite electrical conductivity and distilled water box respectively, and the samples are modeled

according to the dimensions in Fig. 3(a) and 3(b). The measured and simulated results of the basic characteristics of the hydrogel/LM dipole antenna are shown in Fig. 3(d) and 3(e), where the solid line shows the measured results and the dashed line shows the simulated results. Figure 3(d) shows the response characteristics of the sample for different frequencies in the  $0.65\,\mathrm{GHz}$  -  $1.25\,\mathrm{GHz}$  range. It can be seen that the  $S_{11}$  value of the sample without LM is close to 0, and the S<sub>11</sub> curve is consistent with the simulation results. For the sample with LM, the measured  $f_0$  is 0.9275 GHz and  $S_{11}$  is - 12.6 dB, which is close to the simulated result of  $f_0$  is 0.9610 GHz and S<sub>11</sub> is - 13.6 dB. The comparative experimental results show that the hydrogel reflects almost all of the incident electromagnetic wave energy, while the LM dipole antenna radiates most of the incident electromagnetic wave effectively into free space. Figure 3(e) shows the normalized radiation patterns of the hydrogel/LM dipole antenna at 0.9 GHz. As can be seen, the measured E-plane pattern shows an "8" shape and the H-plane pattern shows a circle. The radiation direction of the dipole antenna exhibits an omnidirectional radiation pattern in free space, which is consistent with the simulation results. The difference between the simulated and measured results may be due to the influence of fabrication errors and residual LM in the path of the needle withdrawal from the hydrogel as shown in Fig. 3(b). The simulated radiation gain and efficiency of the proposed antenna are plotted in Fig. 3(f). Result shows that the gain and efficiency are 2 dBi and 52%, respectively, at 0.9 GHz. In order to further investigate the radiation mechanism of the proposed antenna, surface current distribution at 0.9 GHz is plotted in Fig. 3(g). It can be seen that two current peaks appear symmetrically in the middle of the dipole resulting in a resonance.

## 3.2. Influence of parameters on the frequency property of hydrogel/LM dipole antenna

#### 3.2.1. Effect of LM-dipole length

We recorded and characterized the frequency properties of the dipole antenna with different lengths in the free space position. Each antenna branch is formed by injecting LM into the  $0.6\,\mathrm{mm}$  width and  $0.2\,\mathrm{mm}$  thickness microchannels symmetrically inscribed by femtosecond laser in the central axis of the 8 mm width and 7 mm thickness hydrogel slab. After LM injection, the dipole lengths are  $0, 40, 50, 60, \mathrm{and}\ 70\,\mathrm{mm}$ , and the hydrogel lengths are cut into  $40, 60, 70, 80, \mathrm{and}\ 90\,\mathrm{mm}$  according to the dipole lengths, forming the hydrogel/LM dipole antenna. The measured reflection coefficients  $S_{11}$  of hydrogel/LM dipole antennas with different lengths are shown in Fig. 4. It can be seen that the  $S_{11}$  curve of no LM ( $0\,\mathrm{mm}$  length) approaches  $0\,\mathrm{dB}$ , indicating that the sample hardly radiates. In the case of LM dipole length increases from  $40\,\mathrm{mm}$  to  $50\,\mathrm{mm}$ ,  $60\,\mathrm{mm}$ , and  $70\,\mathrm{mm}$ , the measured  $f_0$  decreases from  $1.0133\,\mathrm{GHz}$  to  $0.9442\,\mathrm{GHz}, 0.8982\,\mathrm{GHz}$ , and  $0.7372\,\mathrm{GHz}$ , and the corresponding  $S_{11}$  increase from  $-10.6\,\mathrm{dB}$  to  $-9.4\,\mathrm{dB}$ ,  $-9.1\,\mathrm{dB}$ , and  $-8.0\,\mathrm{dB}$ . Results show that the hydrogel/LM dipole antenna  $f_0$  decreases with increasing dipole length, which is consistent with the theoretical dipole antenna  $f_0$  variation with length [60]. The  $S_{11}$  increases with the increase of hydrogel/LM dipole length, indicating the return loss increases.

#### 3.2.2. Effect of LM-dipole width

Figure 5 shows the frequency properties of the dipole antenna at different widths in the free space position. Each antenna branch is prepared by injecting LM into the 24 mm length and 0.2 mm thickness microchannels symmetrically inscribed by femtosecond laser in the middle of the 70 mm  $\times$  8 mm  $\times$  4 mm hydrogel slab, forming the hydrogel/LM dipole antenna. The measured S<sub>11</sub> of hydrogel/LM dipole antennas with different widths are shown in Fig. 5. It can be seen, as the width increases from 0.5 mm to 1.0 mm, 1.5 mm, 2.0 mm, and 2.5 mm, the measured  $f_0$  increased from 1.0838 GHz to 1.1835GHz, 1.2548 GHz, 1.3260 GHz, and 1.3688 GHz, and the corresponding S<sub>11</sub> changed from - 2.9 dB to - 6.0 dB, - 3.8 dB, - 4.9 dB, and - 5.0 dB. Results show that the hydrogel/LM dipole antenna  $f_0$  increases with increasing dipole width. Considering the measured S<sub>11</sub> value of the antennas, 1 mm was applied as the dipole width for further study.

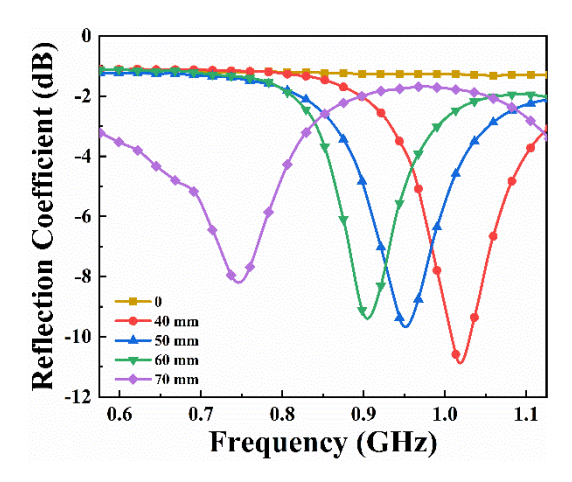


**Fig. 4.** Measured  $S_{11}$  of hydrogel/LM dipole antenna with different lengths. With the increased lengths from 40 to 70 mm, the resonant frequency decreases from 1.0133 to 0.7372 GHz.

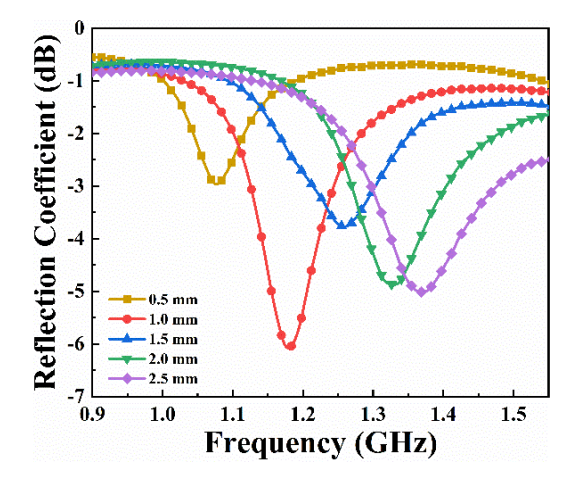


**Fig. 5.** Measured  $S_{11}$  of hydrogel/LM dipole antenna with different widths. With the increased widths from 0.5 to 2.5 mm, the resonant frequency increases from 1.0838 to 1.3688 GHz.

#### 3.2.3. Effect of hydrogel thickness

Figure 6 shows the frequency properties of the dipole antenna with different hydrogel thicknesses. Each LM dipole of  $24~\text{mm} \times 1~\text{mm} \times 0.2~\text{mm}$  is symmetrically embedded in the middle of the  $70~\text{mm} \times 8~\text{mm} \times 4~\text{mm}$  hydrogel slab, forming the hydrogel/LM dipole antenna. The hydrogel thickness is changed by symmetrically attaching the hydrogel film from the direction of the antenna thickness.

The measured  $S_{11}$  of hydrogel/LM dipole antennas in different hydrogel thicknesses are shown in Fig. 6. It can be seen, as the hydrogel thickness increased from 4 to 7 mm, 10 mm, 13 mm, and 16 mm, the measured  $f_0$  decreased from 1.1978 to 1.0836 GHz, 0.9698 GHz, 0.8843 GHz, and 0.8130 GHz, and the corresponding  $S_{11}$  decrease from - 5.7 dB to - 7.5 dB, - 9.7 dB, - 13.2 dB, and - 16.7 dB. Results show that the hydrogel/LM dipole antenna  $f_0$  decreases with the increase of the hydrogel thickness, which is consistent with the theoretical antenna  $f_0$  variation with the effective permittivity of the dielectric substrates [60]. Therefore, the increase in hydrogel

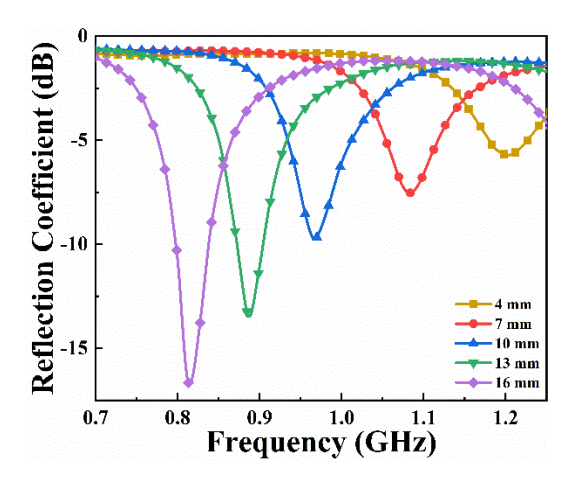


**Fig. 6.** Measured  $S_{11}$  of hydrogel/LM dipole antenna with different thicknesses of the hydrogel. With the increased thickness from 4 to 16 mm, the resonant frequencies decrease from 1.1978 to 0.8130 GHz.

thickness increases the effective permittivity of the substrates where the LM-dipole antenna is located. It can be reasonably supposed that at a certain frequency, the antenna length will be downsized by increasing the hydrogel thickness, which is beneficial for antenna miniaturization.

#### 3.3. Stretchability and tunability of hydrogel/LM dipole antenna

To stretch the antenna, an apparatus consisting of two plastic clamps on a displacement table onto which the ends of the antenna are fixed. The clamps are driven by a manual displacement table, parallel to the long axis of the antenna. The device does not contain metallic parts to avoid electronic coupling with the antenna, thus simplifying the interpretation of the results. Two LM-dipole ( $24 \text{ mm} \times 1 \text{ mm} \times 0.2 \text{ mm}$ ) symmetrically are embedded in the middle of a hydrogel slab ( $80 \text{ mm} \times 8 \text{ mm} \times 4 \text{ mm}$ ), forming the hydrogel/LM dipole antenna. The antenna is stretched from 50 to 74 mm (defined as the total end-to-end length of the LM dipole) because it minimized the chances of tearing the device (discussed below).

We recorded the frequency and length of the antenna at 3 mm increments, but only plotted four series for clarity in Fig. 7. Figure 7(a) shows that elongating the antenna modulates the frequency response. It can be seen that the unstrained antenna resonated at approximately 0.9270 GHz and exhibited an S<sub>11</sub> value of -5.0 dB. As the tensile strain of the antenna increases from 12% to 24%, 36%, and 48%,  $f_0$  decreased from 0.8843 GHz to 0.8415 GHz, 0.7988 GHz, and 0.7703 GHz; correspondingly, S<sub>11</sub> decreases from - 5.4 dB to - 7.0 dB, - 7.1 dB, and -7.8 dB. The results show that both the antenna's  $f_0$  and  $S_{11}$  decrease with increasing tensile strain. It indicates that the return loss of flexible antenna prepared by this method can be partly compensated by stretching. By repeatedly stretching it up to  $\sim 50\%$  strain, the flexible antenna's  $f_0$  and  $S_{11}$  are shown in Fig. 7(b), with error bars indicating their deviations in 3 repetitions. It can be seen that the antenna's  $f_0$  decreases approximately linearly with increasing tensile strain, and both the antenna's  $f_0$  and  $S_{11}$  almost return to their initial values after releasing the strain. Therefore, the 5-cm-long hydrogel/LM dipole antenna prepared by this method can be tuned in the frequency range of 0.7703 GHz to 0.9270 GHz by varying the applied strain from 0 to 48%. In addition, the stretchable antenna can also serve as a strain sensor, as it can repeatedly return to its original shape after multiple deformations without electromagnetic properties losing.

When further stretched from 50 to 80%, LM leakage occurred at the bonding interface of the hydrogel and SMA connector, resulting in an almost constant length and finer LM

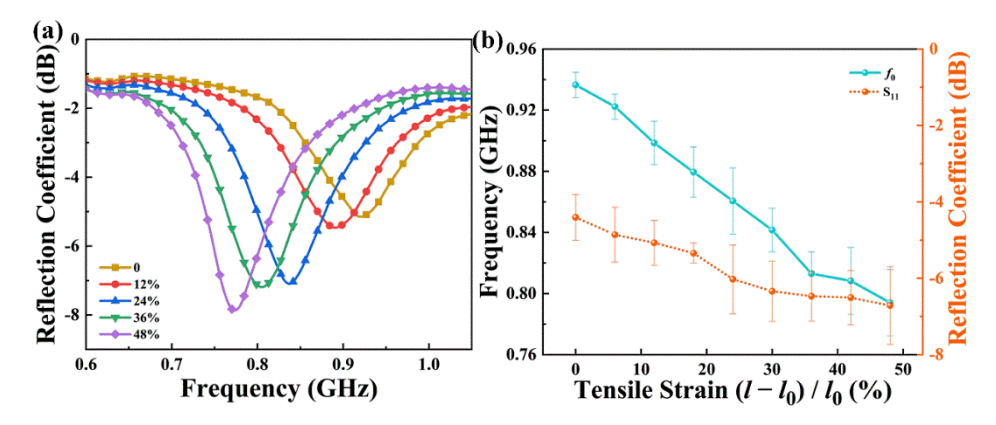


**Fig. 7.** (a) The frequency properties of the hydrogel/LM dipole antenna in its relaxed state (50 mm length) and mechanically elongated states (56, 62, 68, and 74 mm length), and (b) the antenna's  $f_0$  and  $S_{11}$  under stretching for mechanical tuning.

dipole. When the tensile strain exceeds 80%, the hydrogel ruptures at the bonding interface with SMA. It is known that the mechanical properties of LM wires usually depend on the material encapsulating them. In principle, the hydrogel can be stretched up to 1000% strain [70]. However, the hydrogel/LM dipole antenna is much less than 1000% strain, probably because the implantation of rigid SMA into the flexible hydrogel leads to a mismatch of elastic modulus [71] and flaw-sensitivity problem [72], resulting in stress concentration and subsequent breakage of the hydrogel during stretching. This ultimately causes premature failure of the flexible and stretchable antenna before reaching the tensile strain limit of the hydrogel. For improving the stretchability of the hydrogel/LM antenna, a stitch-bonding strategy [73] of hydrogel and SMA metal connectors can be applied by introducing a polymer chain with a versatile functional group and triggerable crosslinking property, which can stitch the hydrogel by forming a network in the topological entanglement with the preexisting hydrogel network. Through this, the polymer chain solution works as a universal glue for the facile adhesion of hydrogels to diverse substrates like metals.

#### 4. Conclusion

In this study, we have developed a new method to build stretchable dipole antennas with tunable resonance frequencies by injecting LM into the femtosecond-laser-inscribed hydrogel microchannels. Measured and simulated results showed that the 5 cm long dipole antenna resonated at approximately 927.5 MHz and exhibit an  $S_{11}$  value of - 12.6 dB. Benefiting from the hydrogel's high permittivity of 79, the dipole antenna length is downsized by half compared with flexible antennas such as PDMS/LM at the same  $f_0$ , realizing the miniaturization of the antenna. By increasing the hydrogel thickness and optimizing the structural parameters, the length of the hydrogel/LM antenna can be reduced and match up to the required  $S_{11}$  parameters. In addition, the 5 cm long hydrogel/LM dipole antenna  $f_0$  can be tuned in the range of 770.3 MHz - 927.0 MHz within the 0 - 48% strain range. This method provides a simple and scalable technique for the design and preparation of LM-pattern microstructures in hydrogels and has potential applications in hydrogel-based soft electronic device.

**Funding.** National Natural Science Foundation of China (62027822); National Key Research and Development Program of China (2017YFB1104600).

**Acknowledgments.** The authors thank Feng Xiang (Xi'an Jiaotong University, China) for help in measuring and discussing the dielectric properties of hydrogels.

**Disclosures.** The authors declare no conflicts of interest.

**Data availability.** Data underlying the results presented in this paper are not publicly available at this time but may be obtained from the authors upon reasonable request.

#### References

- M. Alibakhshikenari, B. S. Virdee, C. H. See, P. Shukla, S. Mansouri Moghaddam, A. U. Zaman, S. Shafqaat, M. O. Akinsolu, B. Liu, J. Yang, R. Abd-Alhameed, F. Falcone, and E. Limiti, "Dual-Polarized highly folded bowtie antenna with slotted self-grounded structure for Sub-6 GHz 5 G applications," IEEE Trans. Antennas Propag. 70(4), 3028–3033 (2022).
- I. Nadeem, M. Alibakhshikenari, F. Babaeian, A. A. Althuwayb, B. S. Virdee, L. Azpilicueta, S. Khan, I. Huynen, F. Falcone, T. A. Denidni, and E. Limiti, "A comprehensive survey on 'circular polarized antennas' for existing and emerging wireless communication technologies," J. Phys. D: Appl. Phys. 55(3), 033002 (2022).
- M. Alibakhshikenari, B. S. Virdee, P. Shukla, C. H. See, R. A. Abd-Alhameed, F. Falcone, and E. Limiti, "Improved adaptive impedance matching for RF front-end systems of wireless transceivers," Sci. Rep. 10(1), 14065 (2020).
- W. A. Awan, S. I. Naqvi, W. A. E. Ali, N. Hussain, A. Iqbal, H. H. Tran, M. Alibakhshikenari, and E. Limiti, "Design and realization of a frequency reconfigurable antenna with wide, dual, and single-band operations for compact sized wireless applications," Electronics 10(11), 1321 (2021).
- M. Alibakhshi-Kenari, M. Naser-Moghadasi, R. A. Sadeghzadeh, B. S. Virdee, and E. Limiti, "A new planar broadband antenna based on meandered line loops for portable wireless communication devices," Radio Sci. 51(7), 1109–1117 (2016).
- M. Alibakhshi-Kenari, A. Andújar, and J. Anguera, "New compact printed leaky-wave antenna with beam steering," Microw. Opt. Technol. Lett. 58(1), 215–217 (2016).
- M. Alibakhshi-Kenari, M. Naser-Moghadasi, R. A. Sadeghzadeh, B. S. Virdee, and E. Limiti, "Bandwidth extension
  of planar antennas using embedded slits for reliable multiband RF communications," AEU International Journal of
  Electronics and Communications 70(7), 910–919 (2016).
- X. Wang, Z. Liu, and T. Zhang, "Flexible sensing electronics for wearable/Aattachable health monitoring," Small 13(25), 1602790 (2017).
- Z. Xie, R. Avila, Y. Huang, and J. A. Rogers, "Flexible and stretchable antennas for biointegrated electronics," Adv. Mater. 32(15), 1902767 (2020).
- M. A. S. M. Al-Haddad, N. Jamel, and A. N. Nordin, "Flexible antenna: A review of design, materials, fabrication, and applications," J. Phys.: Conf. Ser. 1878(1), 012068 (2021).
- D. H. Kim, R. Ghaffari, N. Lu, and J. A. Rogers, "Flexible and stretchable electronics for biointegrated devices," Annu. Rev. Biomed. Eng. 14(1), 113–128 (2012).
- S. Zhao, J. Li, D. Cao, G. Zhang, J. Li, K. Li, Y. Yang, W. Wang, Y. Jin, R. Sun, and C. P. Wong, "Recent advancements in flexible and stretchable electrodes for electromechanical sensors: strategies, materials, and features," ACS Appl. Mater. Interfaces 9(14), 12147–12164 (2017).
- I. Jeerapan and S. Poorahong, "Review-Flexible and stretchable electrochemical sensing systems: materials, energy sources, and integrations," J. Electrochem. Soc. 167(3), 037573 (2020).
- J.-H. So, J. Thelen, A. Qusba, G. J. Hayes, G. Lazzi, and M. D. Dickey, "Reversibly deformable and mechanically tunable fluidic antennas," Adv. Funct. Mater. 19(22), 3632–3637 (2009).
- 15. S. Cheng and Z. Wu, "A microfluidic, reversibly stretchable, large-area wireless strain sensor," Adv. Funct. Mater. **21**(12), 2282–2290 (2011).
- 16. M. A. Kenari, "Printed planar patch antennas based on metamaterial," International Journal of Electronics Letters **2**(1), 37–42 (2014).
- M. Alibakhshikenari, B. S. Virdee, C. H. See, R. A. Abd-Alhameed, F. Falcone, and E. Limiti, "Super-Wide Impedance Bandwidth Planar Antenna for Microwave and Millimeter-Wave Applications," Sensors 19(10), 2306 (2019).
- M. Alibakhshi-Kenari, M. Naser-Moghadasi, and R. A. Sadeghzadeh, "Composite right-left-handed-based antenna with wide applications in very-high frequency-ultra-high frequency bands for radio transceivers," IET Microwaves, Antennas & Propagation 9(15), 1713–1726 (2015).
- M. Alibakhshi-Kenari, M. Naser-Moghadasi, B. S. Virdee, A. Andújar, and J. Anguera, "Compact antenna based on a composite right/left-handed transmission line," Microw. Opt. Technol. Lett. 57(8), 1785–1788 (2015).
- 20. M. Alibakhshikenari, B. S. Virdee, S. Salekzamankhani, S. Aissa, C. H. See, N. Soin, S. J. Fishlock, A. A. Althuwayb, R. Abd-Alhameed, I. Huynen, J. A. McLaughlin, F. Falcone, and E. Limiti, "High-isolation antenna array using SIW and realized with a graphene layer for sub-terahertz wireless applications," Sci. Rep. 11(1), 10218 (2021).
- 21. M. Alibakhshikenari, B. S. Virdee, C. H. See, P. Shukla, S. Salekzamankhani, R. A. Abd-Alhameed, F. Falcone, and E. Limiti, "Study on improvement of the performance parameters of a novel 0.41-0.47 THz on-chip antenna based on metasurface concept realized on 50 mum GaAs-layer," Sci. Rep. 10(1), 11034 (2020).
- R. Guo, J. Tang, S. Dong, J. Lin, H. Wang, J. Liu, and W. Rao, "One-step liquid metal transfer printing: Toward fabrication of flexible electronics on wide range of substrates," Adv. Mater. Technol. 3(12), 1800265 (2018).
- 23. Y. Wang, C. Yan, S. Y. Cheng, Z. Q. Xu, X. Sun, Y. H. Xu, J. J. Chen, Z. Jiang, K. Liang, and Z. S. Feng, "Flexible RFID tag metal antenna on paper-based substrate by inkjet printing technology," Adv. Funct. Mater. 29(29), 1902579 (2019).

- S. Cheng, A. Rydberg, K. Hjort, and Z. Wu, "Liquid metal stretchable unbalanced loop antenna," Appl. Phys. Lett. 94(14), 144103 (2009).
- Y. Zhang, Z. Huo, X. Wang, X. Han, W. Wu, B. Wan, H. Wang, J. Zhai, J. Tao, C. Pan, and Z. L. Wang, "High
  precision epidermal radio frequency antenna via nanofiber network for wireless stretchable multifunction electronics,"
  Nat. Commun. 11(1), 5629 (2020).
- 26. J. Zhang, K. Zhang, J. Yong, Q. Yang, Y. He, C. Zhang, X. Hou, and F. Chen, "Femtosecond laser preparing patternable liquid-metal-repellent surface for flexible electronics," J. Colloid Interface Sci. 578, 146–154 (2020).
- X. Liu, Y. Cao, K. Zheng, Y. Zhang, Z. Wang, Y. Chen, Y. Chen, Y. Ma, and X. Feng, "Liquid droplet stamp transfer printing," Adv. Funct. Mater. 31(52), 2105407 (2021).
- R. Zheng, Z. Peng, Y. Fu, Z. Deng, S. Liu, S. Xing, Y. Wu, J. Li, and L. Liu, "A novel conductive core-shell particle based on liquid metal for fabricating real-time self-repairing flexible circuits," Adv. Funct. Mater. 30(15), 1910524 (2020)
- A. Vásquez Quintero, R. Arai, Y. Yamazaki, T. Sato, and H. De Smet, "Near-field communication powered hydrogel-based smart contact lens," Adv. Mater. Technol. 5(12), 2000702 (2020).
- 30. P. Sen, S. N. R. Kantareddy, R. Bhattacharyya, S. E. Sarma, and J. E. Siegel, "Low-cost diaper wetness detection using hydrogel-based RFID tags," IEEE Sens. J. 20(6), 3293–3302 (2020).
- 31. J. Zhang, J. Yong, C. Zhang, K. Zhang, Y. He, Q. Yang, X. Hou, and F. Chen, "Liquid metal-based reconfigurable and repairable electronics designed by a femtosecond laser," ACS Appl. Electron. Mater. 2(8), 2685–2691 (2020).
- Y. Yu, T. Nguyen, P. Tathireddy, S. Roundy, and D. J. Young, "An in-vitro study of wireless inductive sensing and robust packaging for future implantable hydrogel-based glucose monitoring applications," IEEE Sens. J. 20(4), 2145–2155 (2020).
- S. Lin, H. Yuk, T. Zhang, G. A. Parada, H. Koo, C. Yu, and X. Zhao, "Stretchable hydrogel electronics and devices," Adv. Mater. 28(22), 4497–4505 (2016).
- K.-I. Jang, K. Li, and H. U. Chung, et al., "Self-assembled three dimensional network designs for soft electronics," Nat. Commun. 8(1), 15894 (2017).
- F. Ye, M. Li, D. Ke, L. Wang, and Y. Lu, "Ultrafast self-healing and injectable conductive hydrogel for strain and pressure sensors," Adv. Mater. Technol. 4(9), 1900346 (2019).
- 36. Y. Wang, S. Gong, S. J. Wang, G. P. Simon, and W. Cheng, "Volume-invariant ionic liquid microbands as highly durable wearable biomedical sensors," Mater. Horiz. 3(3), 208–213 (2016).
- 37. E. Bury, S. Chun, and A. S. Koh, "Recent advances in deformable circuit components with liquid metal," Adv. Electron. Mater. 7(4), 2001006 (2021).
- 38. N. Lazarus, C. D. Meyer, S. S. Bedair, H. Nochetto, and I. M. Kierzewski, "Multilayer liquid metal stretchable inductors," Smart Mater. Struct. 23(8), 085036 (2014).
- N. Lazarus and C. D. Meyer, "Stretchable inductor with liquid magnetic core," Mater. Res. Express 3(3), 036103 (2016).
- I. D. Joshipura, H. R. Ayers, C. Majidi, and M. D. Dickey, "Methods to pattern liquid metals," J. Mater. Chem. C 3(16), 3834–3841 (2015).
- 41. Y. H. Wu, Z. F. Deng, Z. F. Peng, R. M. Zheng, S. Q. Liu, S. T. Xing, J. Y. Li, D. Q. Huang, and L. Liu, "A novel strategy for preparing stretchable and reliable biphasic liquid metal," Adv. Funct. Mater. 29(36), 1903840 (2019).
- 42. X. P. Hao, C. Y. Li, C. W. Zhang, M. Du, Z. Ying, Q. Zheng, and Z. L. Wu, "Self-shaping soft electronics based on patterned hydrogel with stencil-printed liquid metal," Adv. Funct. Mater. 31(47), 2105481 (2021).
- 43. R. Guo, X. Wang, H. Chang, W. Yu, S. Liang, W. Rao, and J. Liu, "Ni-GaIn Amalgams enabled rapid and customizable fabrication of wearable and wireless healthcare electronics," Adv. Eng. Mater. 20(10), 1800054 (2018).
- 44. C. Xu, B. Ma, S. Yuan, C. Zhao, and H. Liu, "High-resolution patterning of liquid metal on hydrogel for flexible, stretchable, and self-healing electronics," Adv. Electron. Mater. 6(1), 1900721 (2020).
- Y. Yu, F. Liu, R. Zhang, and J. Liu, "Suspension 3D printing of liquid metal into self-healing hydrogel," Adv. Mater. Technol. 2(11), 1700173 (2017).
- 46. X. Wang, L. Li, X. Yang, H. Wang, J. Guo, Y. Wang, X. Chen, and L. Hu, "Electrically induced wire-forming 3D printing technology of Gallium-based low melting point metals," Adv. Mater. Technol. 6(11), 2100228 (2021).
- 47. H. Liu, M. Li, C. Ouyang, T. J. Lu, F. Li, and F. Xu, "Biofriendly, stretchable, and reusable hydrogel electronics as wearable force sensors," Small 14(36), 1801711 (2018).
- 48. Y. Liu, T. Yang, Y. Zhang, G. Qu, S. Wei, Z. Liu, and T. Kong, "Ultrastretchable and wireless bioelectronics based on all-hydrogel microfluidics," Adv. Mater. 31(39), 1902783 (2019).
- L. Teng, S. Ye, S. Handschuh-Wang, X. Zhou, T. Gan, and X. Zhou, "Liquid metal-based transient circuits for flexible and recyclable electronics," Adv. Funct. Mater. 29(11), 1808739 (2019).
- K. Y. Liu, Q. Yang, Y. L. Zhao, F. Chen, C. Shan, S. G. He, X. L. Fan, L. Li, X. W. Meng, G. Q. Du, and H. Bian, "Three-dimensional metallic microcomponents achieved in fused silica by a femtosecond-laser-based microsolidifying process," Microelectron. Eng. 113, 93–97 (2014).
- T. Tanaka, A. Ishikawa, and S. Kawata, "Two-photon-induced reduction of metal ions for fabricating three-dimensional electrically conductive metallic microstructure," Appl. Phys. Lett. 88(8), 081107 (2006).
- S. Pradhan, K. A. Keller, J. L. Sperduto, and J. H. Slater, "Fundamentals of laser-based hydrogel degradation and applications in cell and tissue engineering," Adv. Healthc. Mater. 6(24), 1700681 (2017).

- 53. B. Joy, Y. Cai, D. C. Bono, and D. Sarkar, "Cell rover-a miniaturized magnetostrictive antenna for wireless operation inside living cells," Nat. Commun. 13(1), 5210 (2022).
- M. Fallahpour and R. Zoughi, "Antenna miniaturization techniques: A review of topology- and material-based methods," IEEE Antennas Propag. Mag. 60(1), 38–50 (2018).
- S. Singhal and A. K. Singh, "CPW-fed hexagonal sierpinski super wideband fractal antenna," IET Microwaves, Antennas Propagation 10(15), 1701–1707 (2016).
- A. Boukarkar, X. Q. Lin, Y. Jiang, and Y. Q. Yu, "Miniaturized single-feed multiband patch antennas," IEEE Trans. Antennas Propag. 65(2), 850–854 (2017).
- C. F. Yang, C. Y. Hsieh, and C. M. Cheng, "Design small-size and wide-band T-shaped patch antenna on ceramic substrate," *Proc. IEEE*, 2919–2922 (2007).
- 58. T. Inui, H. Koga, M. Nogi, N. Komoda, and K. Suganuma, "A miniaturized flexible antenna printed on a high dielectric constant nanopaper composite," Adv. Mater. 27(6), 1112–1116 (2015).
- 59. S. J. Mazlouman, J. Xing Jie, A. Mahanfar, C. Menon, and R. G. Vaughan, "A reconfigurable patch antenna using liquid metal embedded in a silicone substrate," IEEE Trans. Antennas Propag. 59(12), 4406–4412 (2011).
- M. Kubo, X. Li, C. Kim, M. Hashimoto, B. J. Wiley, D. Ham, and G. M. Whitesides, "Stretchable microfluidic radiofrequency antennas," Adv. Mater. 22(25), 2749–2752 (2010).
- H. Guo, L. Shi, M. Yang, J. Wang, R. Yang, S. Qu, and T. Lu, "Highly stretchable and transparent dielectric gels for high sensitivity tactile sensors," Smart Mater. Struct. 28(2), 024003 (2019).
- Z. Zhao, L. Zhang, and H. Wu, "Hydro/Organo/Ionogels: "Controllable" Electromagnetic Wave Absorbers," Adv. Mater. 34(43), 2205376 (2022).
- 63. Y. Gao, J. Song, S. Li, C. Elowsky, Y. Zhou, S. Ducharme, Y. M. Chen, Q. Zhou, and L. Tan, "Hydrogel microphones for stealthy underwater listening," Nat. Commun. 7(1), 12316 (2016).
- R. C. Chiechi, E. A. Weiss, M. D. Dickey, and G. M. Whitesides, "Eutectic gallium-indium (EGaIn): a moldable liquid metal for electrical characterization of self-assembled monolayers," Angew. Chem. Int. Ed. 47(1), 142–144 (2008).
- M. R. Khan, C. Trlica, J. H. So, M. Valeri, and M. D. Dickey, "Influence of water on the interfacial behavior of gallium liquid metal alloys," ACS Appl. Mater. Interfaces 6(24), 22467–22473 (2014).
- 66. A. Hirsch, L. Dejace, H. O. Michaud, and S. P. Lacour, "Harnessing the rheological properties of liquid metals to shape soft electronic conductors for wearable applications," Acc. Chem. Res. 52(3), 534–544 (2019).
- 67. M. D. Dickey, R. C. Chiechi, R. J. Larsen, E. A. Weiss, D. A. Weitz, and G. M. Whitesides, "Eutectic Gallium-Indium (EGaIn): A liquid metal alloy for the formation of stable structures in microchannels at room temperature," Adv. Funct. Mater. 18(7), 1097–1104 (2008).
- B. L. Cumby, G. J. Hayes, M. D. Dickey, R. S. Justice, C. E. Tabor, and J. C. Heikenfeld, "Reconfigurable liquid metal circuits by Laplace pressure shaping," Appl. Phys. Lett. 101(17), 174102 (2012).
- G. J. Hayes, S. Ju-Hee, A. Qusba, M. D. Dickey, and G. Lazzi, "Flexible liquid metal alloy (EGaIn) microstrip patch antenna," IEEE Trans. Antennas Propag. 60(5), 2151–2156 (2012).
- M. A. Haque, T. Kurokawa, and J. P. Gong, "Super tough double network hydrogels and their application as biomaterials," Polymer 53(9), 1805–1822 (2012).
- Z. Li, Z. Liu, T. Y. Ng, and P. Sharma, "The effect of water content on the elastic modulus and fracture energy of hydrogel," Extreme Mechanics Letters 35, 100617 (2020).
- Y. Zhou, J. Hu, P. Zhao, W. Zhang, Z. Suo, and T. Lu, "Flaw-sensitivity of a tough hydrogel under monotonic and cyclic loads," J. Mech. Phys. Solids 153, 104483 (2021).
- Y. Gao, J. Chen, X. Han, Y. Pan, P. Wang, T. Wang, and T. Lu, "A universal strategy for tough adhesion of wet soft material," Adv. Funct. Mater. 30(36), 2003207 (2020).